COMMUNICATIONS IN SCIENCE AND TECHNOLOGY
Homepage: cst.kipmi.or.id

Optimization of an automatic water disposal system based on internet of things to support the smart energy concept

Zulkipli[a,*], Dwi Nurul Huda[b], Muthiah As Saidah[b], Zulfachmi[a], Aggry Saputra[a]

[a]*Department of Informatics Engineering, Sekolah Tinggi Teknologi Indonesia Tanjung Pinang, Tanjungpinang 29122, Indonesia*
[b]*Department of Information Systems, Sekolah Tinggi Teknologi Indonesia Tanjung Pinang, Tanjungpinang 29122, Indonesia*

Article history:
Received: 30 September 2025 / Received in revised form: 5 December 2025 / Accepted: 11 December 2025

Abstract

The management of an Internet of Things (IoT)-based water system powered by solar energy faces significant challenges in achieving high power efficiency and long-term thermal reliability. The objective of this study is to identify the most optimal hardware configuration that balances specific energy efficiency ($\eta_{specific}$) with minimizing thermal energy dissipation in a DC water pumping system. The methodology employed is a comparative experiment that tests six different scenarios, varying the topology of the voltage regulator (Linear Regulator and Buck Converter) and the pump actuator, with a total of 30 pumping cycles at a fixed water volume of 30 litres. The processing of data was undertaken through the utilization of descriptive statistical analysis and Standard Deviation (SD) on the parameters of Power, Temperature, and Water Discharge to measure stability. The findings indicated a critical trade-off between peak energy efficiency and operational stability. Scenario 4 (12V Relay and Mini 560 Buck Converter) emerged as the most optimal configuration, recording the highest Specific Energy Efficiency (1.94 Ws/L). This superiority is evidenced by its excellent thermal stability (36.88°C), which is comparable to that of low-power configurations. In contrast, although Scenario 6 (Synchronous Buck, 51 mm Pump) demonstrated the highest operational stability (Power SD=0.02111), it compromises pumping speed. It is concluded that the implementation of the Mini 560 Buck Converter is imperative in achieving a balance between energy savings and minimizing thermal dissipation, thereby rendering it an ideal selection for solar-powered Smart Energy systems.

Keywords: Specific energy efficiency ($\eta_{specific}$); thermal reliability; smart energy; IoT

1. Introduction

The management of efficient water drainage system is critical, in particular in the context of climate change and elevated rainfall intensity in certain regions [1,2]. The Internet of Things (IoT)-based systems have been extensively implemented as a modern solution for facilitating automated and integrated water management [3]. These systems utilize water level sensors and microcontroller control (NodeMCU ESP32) to drive actuators (DC water pumps), thereby enabling remote intervention through platforms such as Blynk.

However, the power efficiency of these systems remains a major concern [4], particularly given that most of IoT devices rely on renewable energy sources, such as solar panels. DC (direct current) solar power systems require efficient voltage conversion and regulation to supply the microcontroller, which typically operates at 5V or 3.3V, from a 12V source (battery). The power losses (energy dissipation) that occur during this process can reduce the overall system uptime and accelerate component degradation [5].

* Corresponding author. Tel.: +62-819-9120-7990
Email: zulkipli@sttindonesia.ac.id
https://doi.org/10.21924/cst.10.2.2025.1809

Despite the extensive development of solar-powered IoT-based water pumping systems, existing literature overall tends to focus on the enhancement of IoT connectivity or optimization of solar energy harvesting algorithms. A significant research gap exists regarding the specific impact of component selection on the power efficiency of 12V DC systems under dynamic pump loads. Previous studies frequently do not offer a systematic comparison about the disadvantages and advantages of Voltage Regulator Topologies (specifically Linear Regulators vs. Buck Converters) against two critical metrics simultaneously: (1) Specific Energy Efficiency ($\eta_{specific}$) and (2) Thermal Reliability (as measured by component heat dissipation).

To address the issues of operational efficiency and reliability issues, this study proposes an experimental-based approach focused on comparing voltage regulator and pump actuator topologies. Specifically, this study compares the performance of a Linear Regulator (AMS1117), known for its high heat loss, with Buck Converters (Switching Regulators) such as the XL7015, Mini 560, and MP2315, which theoretically offer significantly higher conversion efficiencies [6–8]. Test variations also include relay types (5V and 12V) and different pump capacities, purposely to examine their impact on key

metrics, namely Specific Energy Efficiency ($\eta_{specific}$) and Thermal Resistance.

This approach not only aims to provide a practical solution for the more efficient water management but also contributes to the development of more sustainable Internet of Things (IoT) technologies. Through the optimization of renewable energy utilization, IoT-based wastewater systems have the potential to be an innovative model for addressing challenges and fostering the Smart Energy concept.

2. Research Methods

This study employed a comparative experimental design to evaluate six different hardware configuration scenarios. The entire system was controlled by a NodeMCU ESP32 and powered by a 12-Volt, 45 Ah battery, which was charged via a solar panel and a PWM Solar Charge Controller (SCC).

2.1. Experimental configuration

Test variations, as described in Table 1, were focused on three main components, resulting in six unique scenarios for performance comparison as follows: Step-Down Module (Linear Regulator and Buck Converter), Relay Type (5V and 12V), and Pump Type (Portable Submersible Pump and 51mm Portable Pump). Scenario 1 served as the baseline, by means of a linear regulator and a 5V relay**.**

Table 1. Experiment configuration

Scenario	Relay Type	Step Down Module	Pump Type	Description Variation
Scenario 1 (Baseline)	5V	AMS1117 (Regulator Linear)	Portable Submersible Pump	5V Linear Regulator and 5V Relay
Scenario 2	12V	AMS1117 (Regulator Linear)	Portable Submersible Pump	5V Linear Regulator and 12V Relay
Scenario 3	12V	XL7015 (Buck Converter)	Portable Submersible Pump	Low-power Buck Converter
Scenario 4	12V	Mini 560 (Buck Converter)	Portable Submersible Pump	High-current Buck Converter
Scenario 5	12V	Mini 560 (Buck Converter)	Portable 51mm Pump	Low-power Pump
Scenario 6	12V	MP2315 (Synchronous Buck)	Portable 51mm Pump	High-efficiency Synchronous Buck Converter

2.2. Testing procedures and data collection

Testing was conducted through 30 full pumping cycles for each scenario. Experiments were conducted with a constant water volume of 30 litres in a reservoir, with a reference water level of 20 cm, which served as the operational threshold for the water level sensor. The data recorded in real time included voltage, power, current, cycle time, water flow, and component surface temperature. The main metrics processed included Specific Energy Efficiency ($\eta_{specific}$) (Watt-seconds/Liter) and Surface Temperature (Tavg) as an indicator of Thermal Energy Dissipation. Meanwhile, operational stability was measured using the Standard Deviation (SD) of the main parameters.

Specific Energy Efficiency ($\eta_{specific}$) is defined as the total electrical energy consumed by the system, divided by the volume of water successfully displaced in a single cycle. Given that energy ($E_{electric}$) is the product of power (P) and time (T_{cycle}), and the researcher intended to measure the average active power (P_{avg}) and cycle time (T_{cycle}), a more operational formula is given as follows:

$$\eta_{spesific} = \frac{P_{avg} \cdot T_{cycle}}{V_{pump}} \quad (1)$$

Description:

- P_{avg} = Average system power when the pump is active, in watts (W).
- T_{cycle} = Pumping cycle time (average conversion time) in seconds (s).
- P_{pump} = Experimental water volume (constant 30 litres).

2.3. Circuit visualization

Fig. 1 illustrates the system's functional block diagram, which demonstrates the data control flow through the Wi-Fi Module and the Blynk application. The details of the baseline electrical connections (Scenario 1) are depicted in Fig. 2.

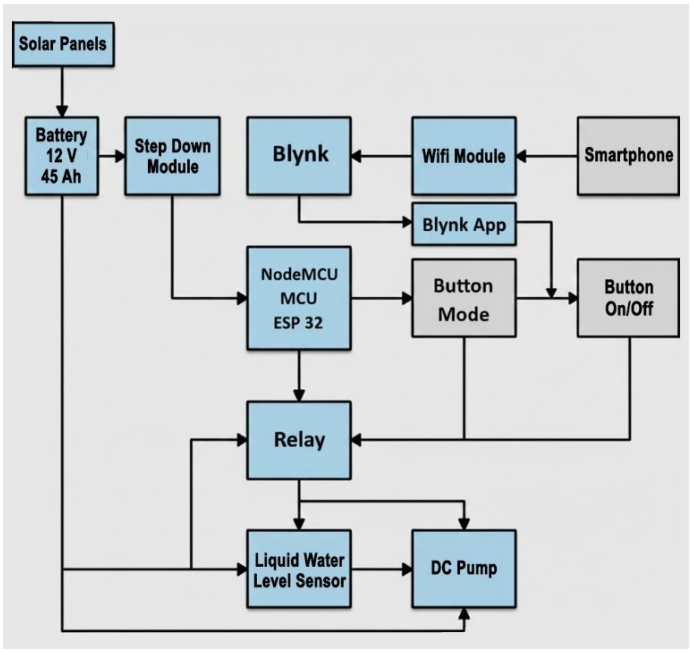

Fig. 1. Functional block diagram of the system

2.4. Data analysis methods

The analysis was conducted by considering several aspects as follows.

- Description of findings. It was conducted by identifying key trends, highest and lowest values, and other important patterns evident in the data.

- Comparisons based on data calculations and performance metrics. If the table contains multiple categories or time periods, the data is then compared purposely to highlight significant differences or similarities.
- Quantitative analysis. It was conducted by calculating averages, percentages, totals, or other relevant metrics to provide a deeper understanding.
- Additional insights. It was conducted to identifying correlations (relationships) between columns, where possible, to provide a more comprehensive insights.

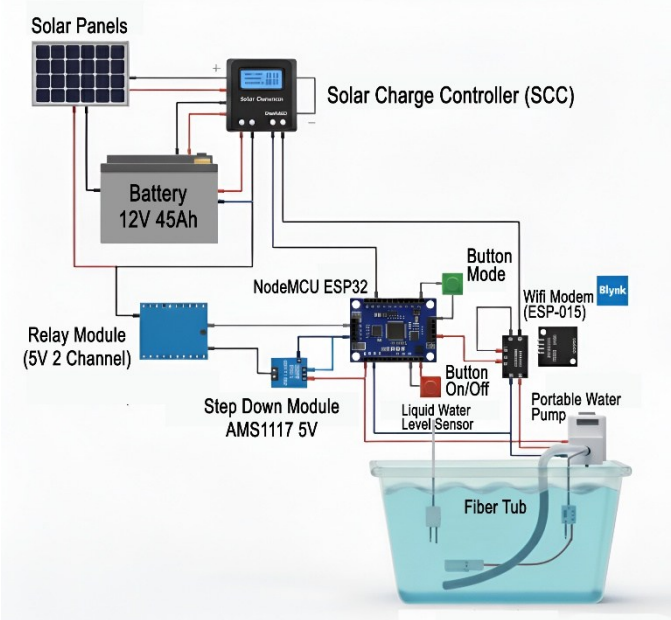

Fig. 2. Device circuit diagram

3. Results and Discussion

The findings of the 30-cycle test demonstrated a significant trade-off between energy efficiency and operational stability, which was grouped by key parameters.

3.1. Performance metrics for Scenario 1

Scenario 1 served as the baseline configuration that employed a 5-Volt Double-Channel Relay and an AMS1117 5-V Step-Down Module (linear regulator) to power the microcontroller. Energy was supplied by a 12-Volt, 45-Ah battery charged by the solar panel through a PWM Solar Charge Controller (SCC). Testing was conducted over 30 full water pumping cycles, with voltage, power, current, cycle time, water flow, and component surface temperature recorded.

Data collected from 30 cycles was processed to obtain average values and calculate key system performance metrics, namely Specific Energy per Litre of Water and Average Power during active conditions (pump on).

As depicted in Table 2, Scenario 1 configuration employed an AMS1117 linear regulator which has been recognized to possess low power conversion efficiency, particularly when the input and output voltage difference is large (e.g. 12V to 5V) [9]. The unconverted energy was converted into heat, which is evident in the average surface temperature value of 37.01°C. Although this temperature value is not extreme, the Step Down component has the potential to be a major source of energy loss (in the form of heat) and impact long-term reliability.

Table 2. Average baseline parameters from Scenario 1 data collection

Parameters	Average Value	Unit
Voltage (V_{avg})	12.24	Volts
Current (I_{avg})	0.11	Amperes
Power (P_{avg})	1.31	Watts
Cycle Time (t_{avg})	44.43	Seconds
Water Flow (Q_{avg})	0.67	Liters/second
Surface Temperature (T_{avg})	37.01	Celsius

3.2. Performance metrics for Scenario 2

Scenario 2 as demonstrated in Table 3 was undertaken by replacing the 5-volt double-channel relay with a 12-volt double-channel relay. The Step-Down Module continued to utilize an AMS1117 5-V linear regulator. This modification aimed to assess the efficiency and reliability impacts by operating the relay coil at the nominal battery voltage (12V), which may result in a reduction of the load on the 5V Step-Down output, but it was also potential to increase the idle power consumption of the 12V line.

Table 3. Average basic parameters of data collection results for Scenario 2

Parameters	Average Value	Unit
Voltage (V_{avg})	12.4	Volts
Current (I_{avg})	0.11	Amperes
Power (P_{avg})	1.36	Watts
Cycle Time (t_{avg})	44.4	Seconds
Water Flow (Q_{avg})	0.68	Liters/second
Surface Temperature (T_{avg})	38.43	Celsius

Table 4. Comparison of Scenario 2 data and Scenario 1

Key Metrics	Scenario 1 (Relay 5V)	Scenario 2 (Relay 12V)	Differences
$\eta_{specific}$ (Watt-second/Liter)	1.95	2	↑0.05
Average Power (W)	1.31	1.36	↑0.05
Volume per Cycle (L)	29.77	30.19	↑0.42
Surface Temperature (°C)	37.01	38.43	↑1.42

In Scenario 2, switching the relay from 5V to 12V demonstrated a slight decrease in specific efficiency (from 1.95 to 2.00 Ws/L) and an average increase in power consumption of 0.05 W. Although the 12V relay should reduce the load on the 5V step-down, which had lower efficiency, this increase in overall power consumption was likely attributable to [10]:

- Higher power consumption of the 12V relay coil in

comparison to the 5V relay coil at the same voltage.

- Significant increase of temperature (1.42°C higher), indicating that the total power losses in the control circuit (including the relay and AMS1117) were found greater in the Scenario 2 configuration. These findings are based on the results of research depicted in Table 4.

3.3. Performance metrics for Scenario 3

Scenario 3 as described in Table 5 represented a crucial step in efficiency testing. It substituted the AMS1117 linear regulator, which was employed in Scenario 1 and Scenario 2 with the XL7015 High Voltage Input DC-DC Adjustable Step-Down Module. The XL7015 employed a switching converter (buck converter) topology, which theoretically offers much higher power conversion efficiency. The relay utilized remained a 12-volt relay, and the pump was a 12-volt DC Portable Submersible Pump.

Table 5. Average basic parameters of data collection results for Scenario 3

Parameters	Average Value	Unit
Voltage (V_{avg})	12.28	Volts
Current (I_{avg})	0.11	Amperes
Power (P_{avg})	1.31	Watts
Cycle Time (t_{avg})	45.07	Seconds
Water Flow (Q_{avg})	0.67	Litres/second
Surface Temperature (T_{avg})	38.16	Celsius

Efficiency ($\eta_{specific}$). Despite its classification as buck converter, the XL7015 exhibited a slightly lower specific efficiency (1.96 Ws/L) in comparison to the baseline Scenario 1 (1.95 Ws/L). This finding indicates that the power losses in the step-down converter may only account for a minor proportion of the total system power consumption during when pump operation. Alternatively, the XL7015 exhibits reduced efficient under very light load conditions (ESP32 supply) compared to the expected performance [11]. However, as illustrated in Table 6, Scenario 3 demonstrated a clear improvement in efficiency in comparison to Scenario 2.

Table 6. Comparison of data with Scenario 3 with the previous one

Key Matrics	Scenario 1 (AMS1117, 5V Relay)	Scenario 2 (AMS1117, 12V Relay)	Scenario 3 (XL7015, 12V Relay)
$\eta_{spesifik}$ (Ws/L)	1.95	2	1.96
Average Power (W)	1.31	1.36	1.31
Surface Temperature (◦C)	37.01	38.43	38.16

Furthermore, the average temperature (38.16°C) in Scenario 3 decreased compared to Scenario 2 (38.43°C). This finding suggests that the implementation of the switching converter (XL7015) successfully reduced heat dissipation (power losses) in the control system, potentially enhancing the long-term reliability of the system when compared to the configuration as observed in Scenario 2.

3.4. Performance metrics for Scenario 4

In Scenario 4 as presented in Table 7 the switching converter exploration was continued by substituting the XL7015 step-down module (from Scenario 3) with a Mini 560 DC-DC Stepdown Buck Converter 5A. The Mini 560 is a buck converter with a higher current capacity, intended to test the effect of maximum current availability and conversion efficiency of high-capacity switching modules. The relay employed was a 12-volt relay, and the pump was a 12-volt DC portable submersible pump.

Table 7. Average basic parameters of data collection results for Scenario 4

Parameters	Average Value	Unit
Voltage (V_{avg})	12.26	Volts
Current (I_{avg})	0.1	Amperes
Power (P_{avg})	1.2	Watts
Cycle Time (t_{avg})	48.88	Seconds
Water Flow (Q_{avg})	0.62	Litres/second
Surface Temperature (T_{avg})	36.88	Celsius

So far, the utilization of the Mini 560 Buck Converter in Scenario 4 produced the optimal specific efficiency. In terms of efficiency ($\eta_{specific}$), Scenario 4 achieved the lowest $\eta_{specific}$ (1.94 Ws/L), indicating the highest power efficiency per litre of water pumped. The average power consumed was also observed at the lowest (1.20W). In Durability (Temperature) scenario, the recorded surface (36.88◦C) was also observed at the lowest among all scenarios, even lower than the baseline Scenario 1. This low temperature indicates minimal power loss in the components, which directly supports the device's long-term reliability criteria. It is worth noting that Scenario 4 exhibited the lowest average water flow (0.62 L/s) and the longest cycle time (48.88 seconds). Nevertheless, the overall energy efficiency remained superior, indicating that the Mini 560 Step Down module provides a highly efficient power supply to the microcontroller, thereby ensuring minimal total system power consumption is minimal [12]. These findings are clearly presented in Table 8.

Table 8. Comparison data with Scenario 4 with the previous scenario

Key Metrics	Scenario 1 (AMS1117)	Scenario 2 (AMS1117)	Scenario 3 (XL7015)	Scenario 4 (Mini 560)
$\eta_{spesifik}$ (Ws/L)	1.95	2	1.96	1.94
Average Power (W)	1.31	1.36	1.31	1.2
Surface Temperature (◦C)	37.01	38.43	38.16	36.88

3.5. Performance metrics for Scenario 5

In Scenario 5 as depicted in Table 9, the impact of substituting the primary actuator (pump) on system performance was examined. The standard portable submersible

pump from the previous scenario was substituted with a 51mm 12V DC portable pump. The control components from Scenario 4 were retained, including the 12-Volt Relay and Mini 560 DC-DC Stepdown Buck Converter. This alteration aimed to evaluate the impact of the pump type on specific energy efficiency and conversion time (cycle time).

Data from 30 cycles were processed to obtain average values and calculate key performance metrics. It should be noted that this data listed Hydraulic Power, indicating that the power consumed by the system is supplied power (electricity), not Hydraulic Power (output). Consequently, the Power (Watts) column from the previous scenario was assumed to be calculated based on $P=V\times I$ at the system input. In Scenario 5, the hydraulic power column would be treated as electrical power (Input), and the analysis would focus on specific energy per liter of water ($\eta_{specific}$).

Table 9. Average basic parameters of data collection results for Scenario 5

Parameters	Average Value	Unit
Voltage (V_{avg})	12.29	Volts
Current (I_{avg})	0.06	Amperes
Power (P_{avg})	0.69	Watts
Cycle Time (t_{avg})	85.98	Seconds
Water Flow (Q_{avg})	0.35	Litres/second
Surface Temperature (T_{avg})	36.78	Celsius

Table 10. Comparison data with Scenario 5 with the previous scenario

Key Metrics	Scenario 4 (Mini 560, Submersible Pump)	Scenario 5 (Mini 560, 51mm Pump)	Key Differences
$\eta_{spesifik}$ (Ws/L)	1.94	1.97	↑0.03 (Slight decrease in efficiency)
Average Power (W)	1.2	0.69	↓0.51 (Very low power)
Cycle Time (t_{avg})	48.88	85.98	↑37.10 (Cycle time almost doubled)
Surface Temperature (°C)	36.88	36.78	↓0.10 (Lowest temperature)

As demonstrated in Table 10, pump replacement in Scenario 5 demonstrated significant alteration in absolute performance parameters. Nevertheless, the specific efficiency remained relatively consistent with the other scenarios. In Scenario 5, the 51 mm portable pump consumed significantly lower average power (0.69 W) when compared to Scenario 4 (1.20 W). However, the average water flow demonstrated a significant decrease (0.35 L/s vs. 0.62 L/s). Consequently, the cycle time increased drastically (85.98 seconds) to move the similar volume of water. Furthermore, despite the very low input power, the specific efficiency of Scenario 5 (1.97 Ws/L) was observed slightly worse than that of Scenario 4 (1.94 Ws/L). This finding suggests that the energy efficiency ratio per litre of the 51 mm pump was slightly lower than that of the portable submersible pump, despite the 51 mm pump requiring less input power. In Scenario 5, its surface temperature (36.78°C) was observed at the lowest among all scenarios, indicating minimal power loss, which provided strong support for the long-term reliability criterion.

3.6. Performance metrics for Scenario 6

In Scenario 6 as presented in Table 11, a configuration that combined a low-power pump (a 51mm Portable 12V DC Pump) from Scenario 5 was tested with another high-efficiency step-down module (the MP2315 3A Mini DC-DC Step Down). The MP2315 is a synchronous buck converter designed for high efficiency, even under light load conditions [13].

Table 11. Average baseline parameters from Scenario 6 data collection

Parameters	Average Value	Unit
Voltage (V_{avg})	12.2	Volts
Current (I_{avg})	0.06	Amperes
Power (P_{avg})	0.74	Watts
Cycle Time (t_{avg})	80.09	Seconds
Water Flow (Q_{avg})	0.37	Liters/second
Surface Temperature (T_{avg})	37.05	Celsius

3.7. Comparison of specific energy efficiency ($\eta_{specific}$) and power stability

As illustrated in Table 2, the $\eta_{specific}$ metric indicated the energy required by the system to move each liter of water, thereby serving as an indicator of the overall system efficiency (control + pump). The lowest value indicates the best efficiency.

Table 12. Comparison of specific energy efficiency ($\eta_{specific}$) and power stability

Scenario	Step Down Module	Pump	$\eta_{spesifik}$ (Ws/L)	P_{avg} (W)	SD Consumption
Scenario 4	Mini 560 (Buck)	Submersible Pump	1.94	1.222	0.13852
Scenario 1	AMS1117 (Linear)	Submersible Pump	1.95	1.3263	0.05654
Scenario 6	MP2315 (Sync Buck)	51mm Pump	2	0.736	0.02111

Scenario 4 recorded the best $\eta_{specific}$ (1.94 Ws/L), confirming that the Mini 560 Buck Converter is an effective means of minimizing power losses in the control circuit. Regarding stability, Scenario 6 demonstrated the smallest power standard deviation (0.02111), indicating the highest operational

consistency, mainly attributable to the minimal power consumption of the pump. As illustrated in Fig. 3, the power trend demonstrated a clear grouping between standard pumps (Scenarios 1-4) and 51mm pumps (Scenarios 5-6)

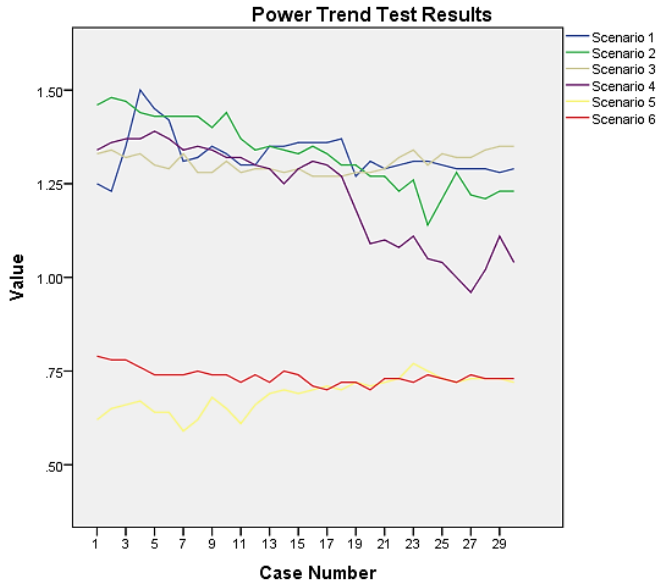

Fig. 3. Trend of test yield power

3.8. Power consumption comparison (mAh)

The metric presented in Table 13 measured the total current drawn from the battery during a 30-cycle test. It served as an indicator of battery performance and smart energy. A lower value was indicative of a longer battery life.

Table 13. Power consumption comparison (mAh)

Scenario	Power Consumption (mAh)	Information
Scenario 2	1192.23	Relay 12V, AMS1117 (Linear)
Scenario 3	1198.97	Relay 12V, XL7015 (Buck)
Scenario 5	1202.35	Relay 12V, Mini 560, Pump 51mm
Scenario 1	1203.95	Relay 5V, AMS1117 (Linear)
Scenario 6	1207.03	Relay 12V, MP2315, Pump 51mm
Scenario 4	1215.57	Relay 12V, Mini 560 (Buck)

As revealed in Scenario 2, the total current consumption was at its lowest point (1192.23 mAh). This finding suggests that, for a system controlled by a 12V relay and AMS1117, the total power loss in the control circuit is lower, thereby directly prolonging the battery lifespan.

3.9. Temperature stability comparison (long-term durability)

As depicted in Table 14, the average surface temperature was directly correlated with the thermal power loss (heat) in the control components (step-down and relay). The reduced temperatures ensure reliability and prolonged component lifespan.

Table 14. Comparison of temperature stability

Scenario	Step Down Module	Pump	Average Temperature (°C)	SD Temperature
Scenario 5	Mini 560 (Buck)	51mm Pump	36.78	0.68666
Scenario 4	Mini 560 (Buck)	Submersible Pump	36.88	1.71331
Scenario 6	MP2315 (Sync Buck)	51mm Pump	37.05	1.18397
Scenario 1	AMS1117 (Linear)	Submersible Pump	37.01	2.68813
Scenario 3	XL7015 (Buck)	Submersible Pump	38.16	1.84348
Scenario 2	AMS1117 (Linear)	Submersible Pump	38.43	1.20629

Thermal Resilience in Scenario 5 exceled in temperature stability (SD=0.68666) and recorded the lowest average temperature (36.8433 ∘C). This low and stable temperature is a key indicator of minimizing thermal energy dissipation. The Temperature Trend (see Fig. 4) demonstrated that the Buck Converter configuration (particularly Scenarios 4, 5, 6) exerted superior thermal stability in comparison to the linear regulator (Scenarios 1 and 2), which experienced elevated temperature spikes.

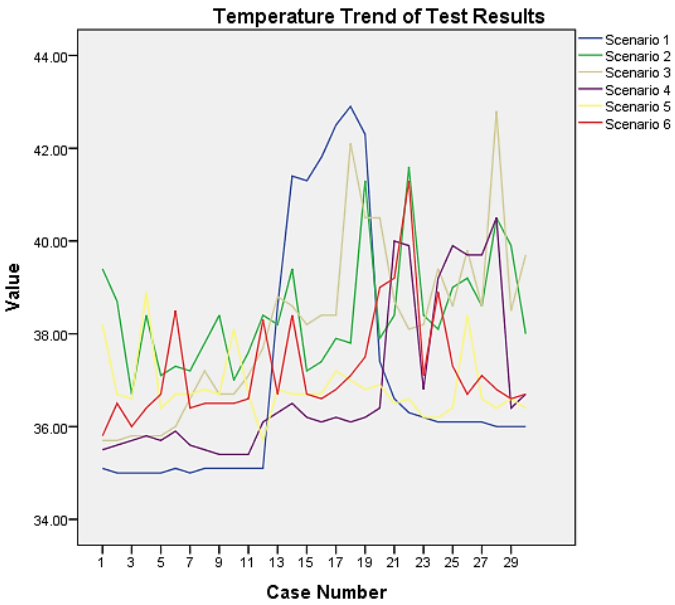

Fig. 4. Device temperature trend

3.10. Contradiction in performance: Water flow rate and specific energy efficiency ($\eta_{specific}$)

The performance evaluation started with the analysis of the trade-off between functional speed (water flow rate) and specific energy efficiency ($\eta_{specific}$). Scenarios 1 and 2, which utilized the Linear Regulator topology, exhibited the highest water flow rate (≈ 0,68 L/second), indicating the fastest response speed. However, this speed was not linearly correlated with energy efficiency. As demonstrated in this study, despite

highly competitive $\eta_{specific}$ values demonstrated in Scenarios 1 and 4 (1,94 Ws/L), Scenario 4 achieved this efficiency with a lower active power draw (1,22 W) and an intrinsically more efficient topology. Nevertheless, a contradiction lied in the failure of Scenarios 5 and 6. Despite the utilization of very low absolute power pumps, a significant decline in water flow rate to 0,35 L/second was observed, thereby severely impeding the system's response speed.

Scientifically, the trade-off between throughput (water flow rate) and energy efficiency has been a subject of discussion in the literature on sensor network. Increased throughput frequently requires higher energy consumption, causing efficiency to not increase linearly [14]. This assertion is further reinforced by Alsalmi et al. who emphasized that the optimization of Mobile Wireless Sensor Networks must consider the balance between energy consumption and network throughput [15]. Nevertheless, extant research indicated that in simultaneous wireless information and power transfer systems, an increase in energy harvesting actually reduces throughput, confirming the presence of an inherent contradiction [16]. Thus, the findings in Scenarios 5 and 6, which exhibited low flow rates despite low absolute power, are consistent with literature emphasizing that energy conversion efficiency is more critical than merely suppressing absolute power.

3.11. Analysis of power dissipation mechanism and thermal reliability implications

The most crucial comparison lies in the Thermal Reliability metric. We discovered that the regulator topology directly determines the system's longevity. The Linear Regulator (AMS1117) in Scenarios 1 and 2 was proven to generate excessive energy dissipation, evidenced by the highest Temperature Standard Deviation (SD) (2,68813°C). Scientifically, the excess voltage ($V_{in} – V_{out}$) is converted into heat, which consistently maintains the operating temperature above the ideal limit. Scenario 4 (Buck Converter Mini 560) demonstrated a complete contrast, maintaining a low average temperature (36,88°C) while simultaneously recording the best $\eta_{specific}$.

Linear regulators such as the AMS1117 are indeed known to generate high level of heat dissipation since the voltage difference is converted into thermal energy. Other research confirmed that linear regulators in industrial IoT applications frequently cause reliability issues in view of excessive heat [17]. Conversely, this finding contradicts research revealing stating that linear regulators are still relevant for simple application needs attributing the stability and affordability of their design [18]. This statement becomes a contradiction as, despite low efficiency, linear regulators are still chosen under certain conditions. On the other hand, several studies have the viewpoint that focusing on the surface properties of lithium ion battery cathodes can also be considered as a strategy to enhance thermal stability [19].

3.12. Comparison of system stability (power SD and water flow rate SD)

To reach a conclusion of the discussion, it is imperative to measure operational stability through the Standard Deviation (SD) of Power and Water Flow Rate SD. Scenario 6 (MP2315) clearly led in terms of stability, with Power SD = 0,02111 W and Water Flow Rate SD = 0,01070 L/second. This enhanced stability is supported by the use of a more advanced Synchronous Buck Converter (MP2315) in controlling output ripple. A contradiction arises when comparing Scenario 4. Although Scenario 4 did not possess the lowest SD, it offered the best $\eta_{specific}$. This finding indicates a profound trade-off: peak stability (Scenario 6) was achieved by sacrificing functional speed and best energy efficiency.

The output stability (Power SD and Water Flow Rate SD) in Scenario 6 aligns with the literature on synchronous buck converters, which can reduce voltage ripple. Research by Ram et al. demonstrated that solar harvesting systems for IoT necessitate low ripple for device stability [20]. However, another study on conductance-based MPPT stated that minor voltage ripple can be tolerated as long as power conversion efficiency remains high [21]. Thus, even though Scenario 4 did not have the optimal stability, its conversion efficiency rendered it superior.

3.13. Justification for balance and optimal solution (Scenario 4)

Based on the multidimensional comparison, Scenario 4 was observed as the most optimal solution. Scenarios 1 and 2 have been eliminated in view of the high risk of thermal reliability; Scenarios 5 and 6 were eliminated due to functional failure (slow speed). Scenario 4 utilized the Buck Converter Mini 560, which was proven capable of balancing the highest $\eta_{specific}$, the lowest operating temperature, and adequate functional speed. The contribution of this research is the identification of this optimal compromise point, affirming that the design of Smart Energy systems must be based on the integration of superior power conversion efficiency with effective thermal management.

The optimal design paradigm for IoT emphasizes the integration of power conversion efficiency with thermal management. Ultra-low power IoT design must combine energy harvesting techniques with heat management to extend device lifespan [22,23]. Zhou et al. also emphasized the importance of transmission power optimization to maintain a balance between energy efficiency and network reliability [24]. However, several studies highlighted that the integration of multi-harvesting can increase system complexity and decrease reliability if not properly managed [25,26]. However, a research states that the AES encryption and decryption methods and algorithms can be modified with the aim of minimizing the resources required for hardware implementation [27].

3.14. Optimal configuration for smart energy and reliability

Based on empirical evidence as explained in Table 15, Scenario 4 is the most comprehensive solution. This scenario fulfilled the Smart Energy criteria through the highest $\eta_{specific}$ and the Long-Term Resilience criteria by minimizing Thermal Energy Dissipation. This balance ensures that the system is not only energy efficient in moving water but also has a long component lifespan, thereby rendering it the most robust choice for a solar-powered IoT-based water disposal system.

Table 15. Comparative matrix of stability and efficiency

Parameters	Scenario 1	Scenario 2	Scenario 3	Scenario 4	Scenario 5	Scenario 6	Information
Efficiency ($\eta_{specific}$) (Ws/L)	1.95	1.99	1.96	1.94 (Best)	2.09	2	Energy per unit volume of water
Average Temperature (°C)	37.0133	38.4267	38.1567	36.88	36.8433 (lowest)	37.24	Thermal Energy Dissipation Indicator
SD Voltage (V)	0.0838	0.08899	0.05522	0.08944	0.01729 (Best)	0.03113	Battery Supply Stability
SD Power (W)	0.05654	0.09358	0.02609	0.13852	0.04521	0.02111 (Best)	Power Consumption Consistency
SD Water Flow (L/sec)	0.02832	0.04727	0.01429	0.07068	0.02266	0.01070 (Best)	Pump Speed Consistency
SD Temperature (°C)	2.68813	1.20629	1.84348	1.71331	0.68666 (Best)	1.18397	Component Thermal Stability
Total Power Consumption (mAh)	1203.95	1192.23 (lowest)	1198.97	1215.57	1202.35	1207.03	Battery Energy Durability Indicator

4. Conclusion

This present study comprehensively evaluated six hardware configuration scenarios, focusing on specific energy efficiency and thermal reliability. Scenario 4 represented the most optimal design. The configuration, combining a 2-Channel 12-Volt Relay and a Mini 560 DC-DC Stepdown Buck Converter with a Portable Submersible Pump, achieved the best Specific Energy Efficiency (1.94Ws/L). This performance was supported by excellent thermal stability (36.88°C), which effectively minimized energy dissipation and ensured long-term device reliability. These results validate that optimal implementation of Buck Converter is imperative to achieving the highest power efficiency in solar-powered IoT systems.

Acknowledgement

The authors wish to express their gratitude for the financial support that made this research possible. This study was funded through the Penelitian Dosen Pemula (PDP) scheme for the fiscal year 2025 by the Direktorat Riset, Teknologi, dan Pengabdian kepada Masyarakat (DRTPM), Direktorat Jenderal Pendidikan Tinggi, Riset, dan Teknologi (BIMA), Ministry of Higher Education, Science, and Technology.

References

1. J. K. Hager, H. R. Mian, G. Hu, K. Hewage, and R. Sadiq, *Integrated planning framework for urban stormwater management: one water approach*, Sustain. Resilient Infrastruct., 8 (2023) 48–69.
2. I. Vargas-Lopez et al., *Assessing Chlorophyll a Spatiotemporal Patterns Combining In Situ Continuous Fluorometry Measurements and Landsat 8/OLI Data across the Barataria Basin (Louisiana, USA),* Water, 13 (2021) 512.
3. S. A. H. AlMetwally, M. K. Hassan, and M. H. Mourad, *Real Time Internet of Things (IoT) Based Water Quality Management System*, Procedia Collège International pour la Recherche en Productique, 91 (2020) 478–485.
4. A. S. Ali, M. N. Abdelmoez, M. Heshmat, and K. Ibrahim, *A solution for water management and leakage detection problems using IoTs based approach*, Internet of Things, 18 (2022) 100504.
5. X. Zhou, P. Giangrande, Y. Ji, W. Zhao, S. Ijaz, and M. Galea, *Insulation for Rotating Low-Voltage Electrical Machines: Degradation, Lifetime Modeling, and Accelerated Aging Tests*, Energies, 17 (2024) 1987.
6. W. Cai and A. Wang, *Research and Design of Microgrid Simulation System Based on Single Chip Microcomputer*, J. Phys. Conf. Ser., 2456 (2023) 012046.
7. A. T. Nugraha, Z. M. Ahmad Putra, M. Santoso, F. Najudah, and M. F. Fathurrohman, *Design of Buck-Boost Converter as A Voltage Stabilizer on Solar Power Plant at PPNS Baruna 01 Crewboat*, E3S Web of Conferences., 473 (2024) 01007.
8. N. N. Pham, J. Leuchter, L. K. Pham, R. Bystřický, and H. Q. Dong, *Battery Monitoring System using Microcontroller ESP32 and Internet of Things*, ECS Transactions., 105 (2021) 517–529.
9. E. M. Diaconu, *Electrical Device Control System Through Wi-Fi Technology*, Sciendo., 21 (2021) 18–21.
10. D. Sharma, R. K. Jain, R. Sharma, B. P. Shan, and O. J. Shiney, *Analysis of BPM/Pulse rate and its correlation with BMI for sprint activity using ATMega328 based Arduino Uno,* Mater. Today Proc.., 80 (2023) 3851–3856.
11. A. Perdomo-Campos, I. Vega-González, and J. Ramírez-Beltrán, *ESP32 Based Low-Power and Low-Cost Wireless Sensor Network,* 2023, Proceedings of 19th Latin American Control Congress 2022,. pp. 275–285.
12. S. Sorin, B. Hnatiuc, M. Hnatiuc, V. Pomazan, and C. Pomazan, *Low drop voltage step-down converter for industrial automation and operation,* Advanced Topics in Optoelectronics, Microelectronics, and Nanotechnologies XI, (2023) 26.
13. H. Luo, H. Wen, X. Li, L. Jiang, and Y. Hu, *Synchronous buck converter based low-cost and high-efficiency sub-module DMPPT PV system under partial shading conditions,* Energy Convers. and Manag., 126 (2016) 473–487.
14. H. Sharma, M. Sharma, C. Sharma, A. Haque, and Z. A. Jaffery, *Performance Analysis of Solar Powered DC-DC Buck Converter for Energy Harvesting IoT Nodes,* in 2018 3rd International Innovative Applications of Computational Intelligence on Power, Energy and Controls with their Impact on Humanity, 2018, pp. 26–29.
15. N. Alsalmi, K. Navaie, and H. Rahmani, *Energy and throughput efficient mobile wireless sensor networks: A deep reinforcement learning approach,* IET Wirel. Sens. Syst., 13 (2024) 413–433.
16. M. Gopal, T. Chandra Prakash, N. Venkata Ramakrishna, and B. P. Yadav, *IoT Based Solar Power Monitoring System,* IOP Conf. Ser. Mater. Sci.

Eng., 981 (2020) 279–283.

17. P.-J. Liu, W.-Y. Cheng, L.-H. Chien, and J.-Y. Lin, *A Fast Transient Current-Mode Buck Converter With Linear Regulation Mode,* IEEE Trans. Power Electron., 38 (2023) 3513–3522.
18. B. Aljafari, P. R. Satpathy, S. B. Thanikanti, and H. Haes Alhelou, *A zero switch and sensorless reconfiguration approach for sustainable operation of roof-top photovoltaic system during partial shading,* IET Renewable Power Generation., 17 (2023) 1385–1412.
19. A. Amri, Y. Bertilsya, Y. Dwi, and S. Pambudi, *Enhancement in thermal stability and surface properties of LiFePO 4 / VFLG composite prepared via sol-gel route,* Commun. Sci. Technol., 10 (2025) 68–74.
20. A. K. Singha, *A Discrete-Time Framework for Designing Stable Digital V^2 Controllers for the Buck Converter,* IEEE Trans. Power Electron., 37 (2022) 14317–14327.
21. T. Binkowski, *A Conductance-Based MPPT Method with Reduced Impact of the Voltage Ripple for One-Phase Solar Powered Vehicle or Aircraft Systems,* Energies, 13 (2020) 1496.
22. E. J. Dzhunusbekov and S. A. Orazbayev, *Electrolytic capacitor life time calculation under varying operating conditions,* Journal of Vibroengineering, 22 (2020) 721–734.
23. Jyothikumari G and Shankar S Miraji, *Ultra-low power design for iot sensors: energy harvesting and power management techniques,* World Journal of Advanced Research and Reviews., 1 (2019) 108–117.
24. C. Zhou, X. Wang, Y. Dou, and X. Chen, *Transmit Power Optimization for Simultaneous Wireless Information and Power Transfer-Assisted IoT Networks with Integrated Sensing and Communication and Nonlinear Energy Harvesting Model,* Entropy, 27 (2025) 456.
25. A. Bothe and A. Balducci, *Thermal analysis of electrical double layer capacitors: Present status and remaining challenges,* J. Power Sources, 548 (2022) 232090.
26. M. Frivaldsky, J. Cuntala, P. Spanik, and A. Kanovsky, *Investigation of thermal effects and lifetime estimation of electrolytic double layer capacitors during repeated charge and discharge cycles in dedicated application,* Electrical Engineering., 100 (2018) 11–25.
27. R. Hadi, S. Arief, S. Madenda, and S. Harmanto, *A modified MixColumn-InversMixColumn in AES algorithm suitable for hardware implementation using FPGA device,* Commun. Sci. Technol., 8 (2023) 198–207.